CIRENE
Air–Sea Interactions in the Seychelles–Chagos Thermocline Ridge Region[*]

BY J. VIALARD,[+] J. P. DUVEL, M. J. MCPHADEN,
P. BOURUET-AUBERTOT, B. WARD,[#] E. KEY, D. BOURRAS,
R. WELLER, P. MINNETT, A. WEILL, C. CASSOU,
L. EYMARD, T. FRISTEDT, C. BASDEVANT,
Y. DANDONNEAU, O. DUTEIL, T. IZUMO,
C. DE BOYER MONTÉGUT, S. MASSON,
F. MARSAC, C. MENKES, AND S. KENNAN

A field experiment in the southwestern Indian Ocean provides new insights into ocean–atmosphere interactions in a key climatic region.

While easterly trade winds blow year-round over the southern Indian Ocean, surface winds experience a striking reversal north of 10°S. During boreal summer, the low-level easterly flow penetrates northward, is deflected when crossing the equator, and forms the strong Indian monsoon jet. During boreal winter, northeasterly winds also bend while crossing the equator southward and form a weak low-level westerly jet between the equator and 10°S (Fig. 1a). The cyclonic circulation at the meeting point of these two wind regimes is responsible for the formation of a peculiar oceanic structure: the "Seychelles Chagos thermocline ridge" (SCTR; Hermes and Reason 2008; see the "Seychelles–Chagos thermocline ridge" sidebar for a more complete explanation of the formation of this feature).

This region has attracted attention because it is home to distinct oceanic and atmospheric variability at multiple time scales, each time with significant climatic consequences. Anomalously warm sea surface temperature (SST) in the SCTR region is associated with increased ▶

Underwater photograph of ASIP. See "The Air–Sea Interaction profiler" sidebar for more information.

cyclonic activity near Madagascar and La Réunion (Jury et al. 1999; Xie et al. 2002). It also induces above-average rainfall along the western Ghats of India during the following monsoon (Vecchi and Harrison 2004; Izumo et al. 2008). Atmospheric model experiments suggest that these SST anomalies force a substantial fraction of interannual precipitation anomalies over the west Pacific and Maritime Continent (Annamalai et al. 2005) and influence the Northern Hemisphere extratropical circulation during boreal winter (Annamalai et al. 2007). These numerous climatic consequences are an incentive to better understand the various climate phenomena that affect SST in this region.

El Niño affects the Indian Ocean in well-known ways. By displacing the western Pacific warm pool and the associated atmospheric deep convection over distances of thousands of kilometers, El Niño disrupts weather patterns at the global scale and can induce SST changes in remote regions via the so-called atmospheric bridge. The Indian Ocean as a whole warms as a response to the surface heat flux perturbations induced by El Niño. However, in the SCTR region, the
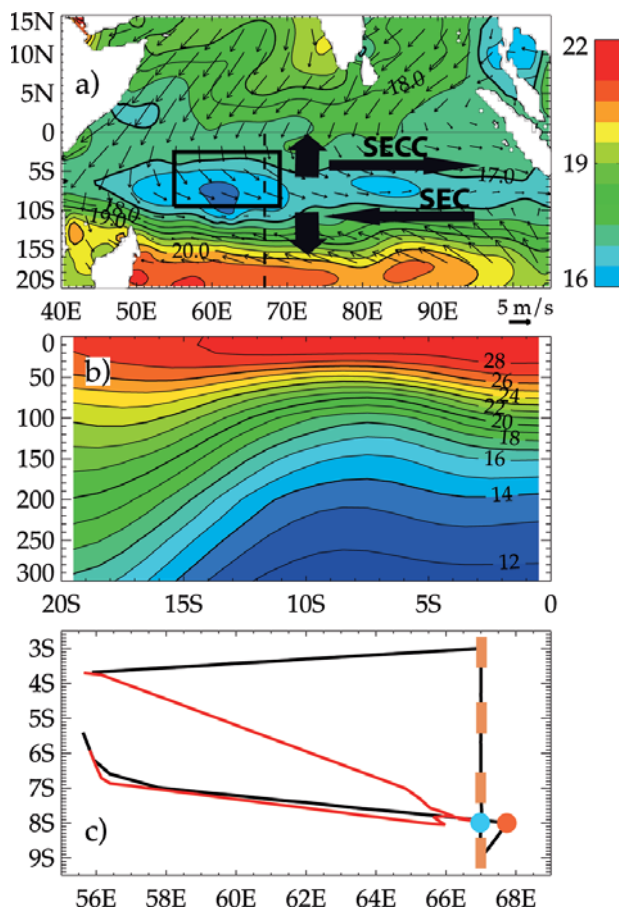

FIG. 1. (a) Climatological surface winds and 0–300-m average ocean temperature in Jan–Feb. (See "The Seychelles–Chagos thermocline ridge" sidebar for explanation.) The thick black arrows indicate the surface flow induced by wind that promotes upwelling and leads to the SCTR formation. The arrows marked SEC and SECC indicate the south equatorial current and south equatorial countercurrent. (b) Meridional section of the ocean temperature along 67°E, indicated by a dashed line in (a). (c) Blowup of the region framed in (a) summarizing the Cirene cruise. The trajectory of R/V *Suroît* is shown in black (first leg) and red (second leg). The orange rectangles indicate the locations where groups of three Argo profilers were deployed. The blue circle indicates the location of the ATLAS and ADCP moorings. The red circle indicates the location of the long CTD station (12 days during each leg). The climatological temperature data come from World Ocean Atlas 2005 (Locarnini et al. 2006), while the wind is the Quick Scatterometer (QuikSCAT) wind gridded product produced by the Center for Satellite Exploitation and Research (CERSAT).

AFFILIATIONS: *VIALARD, BOURUET-AUBERTOT, EYMARD, DANDONNEAU, DUTEIL, MASSON, and MENKES—Laboratoire d'Océanographie Expérimentale et Approches Numériques, CNRS, UPMC, IRD, Paris, France; DUVEL AND BASDEVANT—Laboratoire de Météorologie Dynamique, CNRS, UPMC, ENS, Ecole Polytechnique, Paris, France; MCPHADEN—NOAA/Pacific Marine Environmental Laboratory, Seattle, Washington; +WARD—Old Dominion University, Norfolk, Virginia; KEY, BOURRAS, AND WEILL—Centre d'Etudes des Environnements Terrestres et Planétaires, Vélizy, France; WELLER—Woods Hole Oceanographic Institution, Woods Hole, Massachusetts; MINNETT—University of Miami, Miami, Florida; CASSOU—Centre Européen de Formation Avancée en Calcul Scientifique, Toulouse, France; FRISTEDT—Swedish Defence Research Agency, Stockholm, Sweden; IZUMO AND BOYER MONTÉGUT—Frontier Research Center for Global Change, Yokohama, Japan; MARSAC—IRD, Centre de Recherche Halieutique, Sète, France; KENNAN—NIWA, Wellington, New Zealand

*CURRENT AFFILIATIONS: VIALARD—National Institute of Oceanography, Goa, India
+CURRENT AFFILIATIONS: WARD— National University of Ireland, Galway, Ireland
CORRESPONDING AUTHOR: Dr. Jérôme Vialard, LOCEAN—Case 100, Université Pierre et Marie Curie, 75232 Paris Cedex 05, France.
E-mail: jv@locean-ipsl.upmc.fr

The abstract for this article can be found in this issue, following the table of contents.

observed SST anomalies do not match those induced by El Niño, suggesting that internal ocean dynamics play a role in this region or that they are affected by phenomena other than El Niño (Klein et al. 1999; Lau and Nath 2000).

The Indian Ocean counterpart to El Niño is the Indian Ocean dipole (IOD; e.g., Saji et al. 1999; Webster et al. 1999; Murtugudde et al. 2000). As for El Niño, the IOD is believed to grow as a result of a coupled ocean–atmosphere instability. Imagine that the eastern Indian Ocean cools: the reduced convection will lead to an easterly wind anomaly in the central basin. This wind anomaly drives westward currents at the equator, which lift the thermocline and cool the surface in the east, thus reinforcing the initial anomaly. In 2006, such coupled feedbacks led to a significant cold anomaly in the east and anomalous eastward winds in the central basin (Fig. 2a). The largest IOD anomalies occur during September–November. While the IOD tends to occur simultaneously with El Niño, it can also occur independently.

The IOD has a strong signature in the SCTR region (Vinayachandran et al. 2002), while El Niño–induced variability is strongest south of 10°S (Yu et al. 2005). The eastward wind anomaly associated with the IOD drives southward currents, which accumulate mass and deepen the thermocline to the south, resulting in a strong positive sea level anomaly (Fig. 2b). Under the effects of Earth's rotation, this anomaly propagates westward as oceanic Rossby waves (Masumoto and Meyers 1998). This leads to a deeper thermocline in the SCTR region until April–May the following year (e.g., Fig. 3c in 1998 and 2007). The deeper thermocline results in a diminished connection between subsurface cold waters and the surface, and it causes warm SST anomalies (e.g. Fig. 3c in early 1998 and late 2006). These SST anomalies may feed back to the wind (Xie et al. 2002), potentially making the SCTR the place of a full-fledged air–sea interaction process.

The most striking temperature anomalies in Fig. 3a are not at interannual but at intraseasonal time scales. SST cooling events of 1°–1.5°C, lasting for 1 to 2 months, occurred during the austral summers of 1999–2002, and in 2008. Such events follow by a short lag a sharp increase in atmospheric convective activity (Fig. 3b). These strong cooling events were not noticed by satellite measurements of SST in the infrared window, for which the screening effect of clouds prevents an accurate estimate of ocean cooling below convective systems (Duvel and Vialard 2007). The advent of microwave instruments, like the Tropical Rainfall Measuring Mission (TRMM) Microwave Imager (TMI; Wentz et al. 2000), allowed the links to be highlighted between these SST variations in

THE SEYCHELLES–CHAGOS THERMOCLINE RIDGE

The SCTR is found between 5° and 10°S, to the east of 50°E in the Indian Ocean (Fig. 1a). It corresponds to a region where the thermocline (the sharp vertical temperature gradient between the upper-ocean warm water and deep-ocean colder water) rises close to the surface (Fig. 1b). This year-round feature is more pronounced in boreal winter and can be explained by the surface wind pattern (e.g., McCreary et al. 1993). To the south of the SCTR, easterly winds drive a weak near-surface southward flow (Fig. 1a), because Coriolis force bends the flow toward the left in the Southern Hemisphere. To the north, westerly winds are associated with a near-surface weak northward flow (Fig. 1a). The associated surface divergence is compensated for by an upwelling, which lifts the thermocline and results in this ridge, extending roughly along the northern edge of the easterlies. A more detailed explanation of the formation of this ridge and its annual cycle can be found in Hermes and Reason (2008) and Yokoi et al. (2008).

In most upwelling regions (e.g., the eastern equatorial Pacific or Atlantic), the SST is below 25°C, because of the input of cold thermocline water. The SCTR is quite unique in that surface water is much warmer: above 27°C almost all the time (Fig. 3a) and between 28.5° and 30°C for most of the austral summer. In that temperature range, the atmosphere is very sensitive to small SST variations. Because of the shallow thermocline, the mixed layer is shallow and very responsive to atmospheric heat fluxes (e.g., Duvel et al. 2004), and cold thermocline water can easily by brought to the surface by mixing. It is the combined presence of this shallow thermocline (which promotes SST changes) and the high SST that makes the SCTR a region favorable to strong air–sea interactions (Xie et al. 2002).

The Seychelles–Chagos thermocline ridge also marks the limit between two current systems. Along the SCTR axis, the average water column temperature is colder than to the north and south, and the sea surface is thus depressed (colder water having a smaller specific volume). There is a northward near-surface pressure gradient to the south of the SCTR, which, combined with the effect of the Coriolis force, results in a westward current named the south equatorial current (Fig. 1a; Schott and McCreary 2001). For similar reasons, there is an eastward current, most marked in boreal winter, named the south equatorial countercurrent to the north of the SCTR.
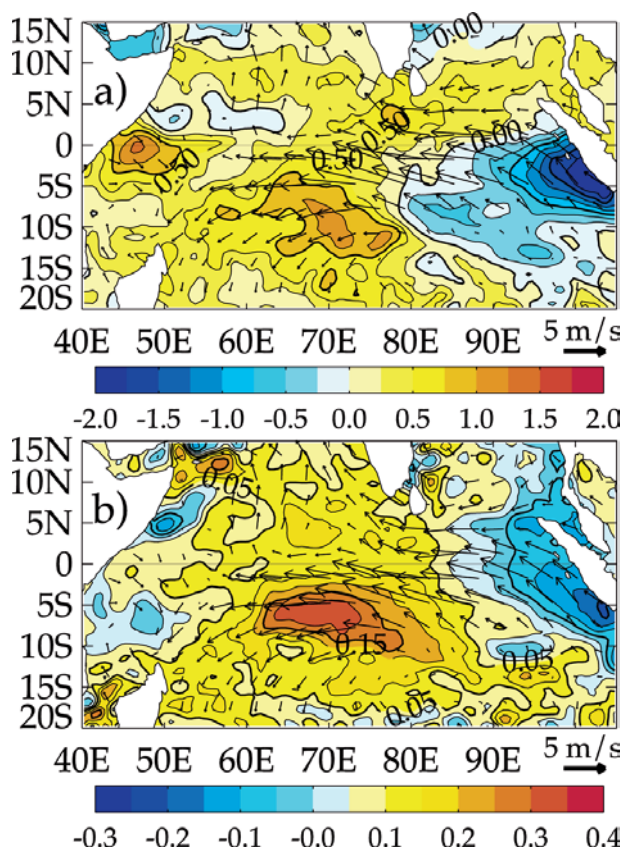
FIG. 2. (a) SST and surface wind anomalies in Nov 2006, at the peak of the Indian Ocean dipole. (b) Sea level (a proxy for the upper-ocean heat content) and surface wind anomalies in Nov 2006. The SST is from TMI (Wentz et al. 2000), while sea level is available from Ssalto/Duacs (www.jason.oceanobs.com/html/donnees/duacs/access_fr.html).

the SCTR region and large-scale perturbations of the convection propagating eastward south of the equator (Harrison and Vecchi 2001; Duvel et al. 2004). This intraseasonal perturbation, with time scales between 30 and 80 days, is known as the Madden–Julian oscillation (MJO; Madden and Julian 1994; Zhang 2005). The MJO explains a large fraction of the variance of tropical convection, and modulates cyclonic activity (increased convection being associated with more cyclones; Liebmann et al. 1994; Bessafi and Wheeler 2006). The MJO convective phase is associated with westerly wind bursts and significant surface flux perturbations (e.g., Duvel et al. 2004). The MJO initially develops over the Indian Ocean and then propagates into the western Pacific, where wind bursts can play a major role in the onset of El Niño events (e.g., McPhaden 1999).

The SCTR is one of the regions of strongest SST intraseasonal variance in the Indo-Pacific warm pool. The shallow thermocline in this region favors the

strong SST response because i) colder water is more readily brought to the surface by upwelling or missing and ii) the mixed layer is constrained to be shallow because of the underlying thermocline and is thus more responsive to atmospheric fluxes (Harrison and Vecchi 2001; Saji et al. 2006; Duvel and Vialard 2007). Modeling studies suggest that considering the MJO surface temperature signature can improve simulations (e.g., Waliser et al. 1999; Maloney and Sobel 2004) and forecasts (Woolnough et al. 2007) of the MJO. The SCTR, with its high surface temperature and strong cooling events, may thus be a key region for understanding the processes responsible for the MJO genesis.

THE VASCO–CIRENE FIELD EXPERIMENT.
The Indian Ocean Panel (IOP) from the CLIVAR project of the World Research Climate Program has stressed that the SCTR should be a major emphasis of the Indian Ocean Observing System (IndOOS; CLIVAR/GOOS IOP et al. 2006). Past observations in the SCTR region include the French *Sinode* cruises from 1979 to 1981 (Fieux and Lévy 1983; Reverdin and Fieux 1987), Russian cruises in 1983 (Plotnikov 1986) and 1987, repeated observations along the so-called IX12 Freemantle–Red Sea commercial line (e.g., Masumoto and Meyers 1998), and a section from the Research Vessel (R/V) *Sonne* in 1993 (Schott et al. 2002). The Vasco–Cirene field experiment is, however, probably the first observational effort in the region dedicated to understanding the strong air–sea interactions at synoptic to interannual time scales in the SCTR. We will mostly present the design of the experiment below. (The interested reader can consult the electronic supplement available from http://dx.doi.org/10.1175/BAMS-12-Vialard for more complete description of the measurements.)

Vasco–Cirene lasted for 2 months (January and February) in 2007. Given the long time scales of phenomena like the MJO or IOD, it was important that Vasco–Cirene not only collected data intensively over this period, but also contributed to the Indian Ocean Observing System in the longer term. The Argo network (Gould et al. 2004) now comprises about 3,100 autonomous units (550 of which are in the Indian Ocean) drifting at 1000-m depth and providing profiles of temperature, salinity, and pressure every 10 days, transmitted to shore via satellite communications. During Cirene, 12 profilers were deployed in groups of three (locations on Fig. 1c). The grouped deployment allowed for good temporal and spatial resolutions during the cruise. After 90 days, the profilers drifted apart from each other and contribute to

the Argo network for their life span of about 3 yr. In collaboration with the Pacific Marine Environmental Laboratory (PMEL), one mooring was also deployed at 8°S, 67°E as a contribution to the research moored array for the African–Asian–Australian Monsoon Analysis and Prediction program (RAMA; McPhaden et al. 2009). The mooring was heavily instrumented for the duration of Vasco–Cirene, and a more lightly instrumented version remained after the cruise and still provides data (see "ATLAS and ADCP moorings at 8°S, 67°E" sidebar for more details). The mooring captured anomalies associated with the end of the 2006 IOD (next section) and the upper ocean signature of strong MJO events in late 2007 and early 2008 (Vialard et al. 2008; see "ATLAS and ADCP moorings at 8°S, 67°E").

The atmospheric deep convection varies strongly in space (from mesoscale to scales of the MJO envelope) and time (from diurnal to intraseasonal). In addition, there is a relatively strong variability of the convection and the MJO activity from one year to another. It is thus difficult to be "at the right place, at the right time" with an oceanographic ship. In the extreme case of cyclone development, there is even a strong incentive to flee away from regions of strong convection. For these reasons, we combined observations from an oceanographic ship (the Cirene cruise, onboard R/V *Suroît*) and observations using meteorological balloons deployed from Mahé in Seychelles (the Vasco experiment). One big advantage of meteorological balloons is that they are attracted toward convective regions by the low-level wind convergence generated by the low surface pressure. As a result, the balloons maximized the number of measurements in the vicinity of active convective systems.

Pressurized balloons and six Aeroclipper prototypes were launched during Vasco. The Aeroclipper is a streamlined balloon, vertically stabilized at ~ 50-m height by a guide rope floating at the ocean surface (see Duvel et al. 2009 for a complete description). As we will see later, several of these balloons were attracted and survived into tropical cyclones.

Air–sea interactions are at the heart of the Vasco–Cirene program. We thus collected both atmospheric and oceanic observations during the cruise, with an emphasis on the upper ocean, atmospheric boundary layer, and air–sea interface. Surface temperature and salinity and currents down to 300 m were continuously recorded, and temperature profiles down to 800 m were collected every 50 km along the ship track (Fig. 1c). Air–sea fluxes were monitored using a dedicated flux platform installed on a mast 17 m above sea surface on the bow of the ship. The mast reduces the impact of the ship structure on the measurements (Dupuis et al. 2003). The platform collected classical meteorological measurements (wind, temperature,
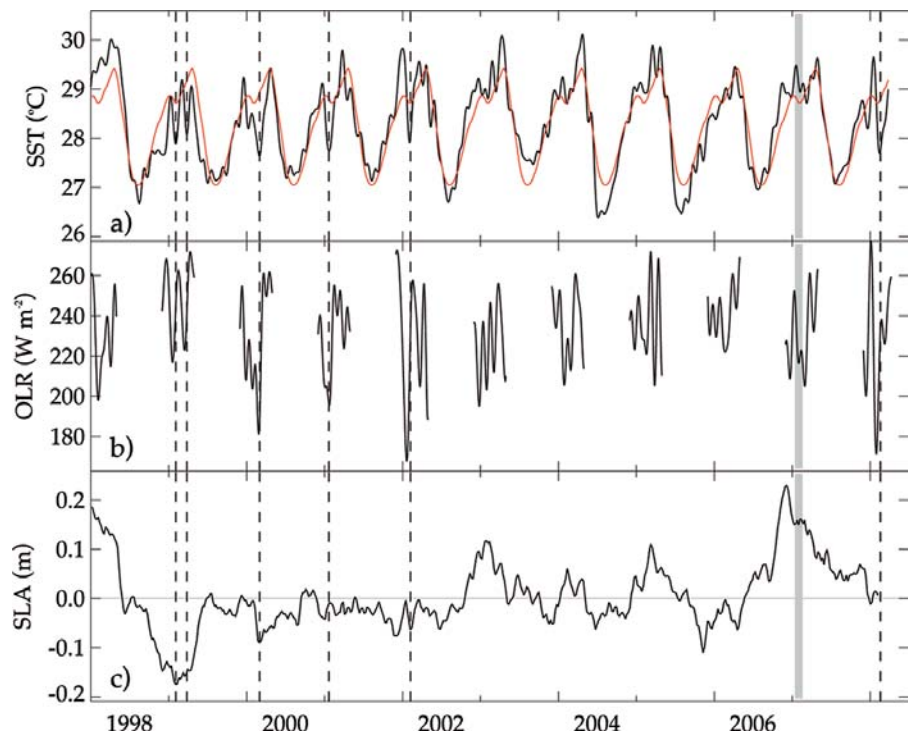

FIG. 3. Time series of average (a) SST, (b) outgoing longwave radiation (OLR; a proxy for convection, low values indicating intense convection), and (c) sea level interannual anomaly over the SCTR region (5°–10°S, 60°–80°E). In (a) and (b) a 30-day low-pass filter has been applied and the climatology is shown in red. Only austral summer OLR is shown to improve readability. The gray bar indicates the timing of the Vasco–Cirene experiment. Dashed lines indicate the strongest intraseasonal SST cooling events. Note that they are associated with sharp increase in atmospheric convection as seen in (b). The OLR is from NOAA (Leibmann and Smith 1996); SST and sea level as in Fig. 2.

ATLAS AND ADCP MOORINGS AT 8°S, 67°E

During Cirene, the R/V *Suroît* deployed a heavily instrumented next-generation ATLAS mooring supplied by the National Oceanic Atmospheric Administration's (NOAA's) PMEL at a nominal location of 8°S, 67°E. The mooring was anchored to the ocean floor in 4,065 m of water depth and was in place for 35 days beginning on 13 January 2007. The purpose of this component of Cirene was to provide high temporal resolution time series data as a complement to other observations during the field campaign to document and diagnose ocean–atmosphere interactions and upper-ocean variability. Measurements included ocean temperature down to 500 m, salinity down to 140 m, and velocity down to 60 m, as well as air temperature, relative humidity, wind velocity, downwelling shortwave and longwave radiation, barometric pressure, and rain rate. Daily averages of most data were transmitted to shore in real time, while high temporal resolution data were internally recorded. A PMEL ADCP mooring was deployed in close proximity to (i.e., within 5.5 nautical miles of) the ATLAS mooring, which provided velocity data between about 20 and 180 m during the field campaign.

The ATLAS and ADCP moorings were recovered on 15 February 2007. The ATLAS mooring was then rede-ployed on 16 February 2007 with a slightly reduced set of instrumentation as a contribution to the RAMA (McPhaden et al. 2009). This mooring was recovered and redeployed in August 2008 by R/V Marion Dufresne. The combination of satellite and in situ measurements from the basin-scale sustained IndOOS (Meyers and Boscolo 2006) moored time series measurements from this ATLAS mooring will provide a long-term climate context for interpretation of the January–February 2007 Cirene cruise observations. For example, the ATLAS mooring allowed for monitoring the upper ocean signature of strong MJOs in late 2007 and early 2008 (Vialard et al. 2008). The surface response to the MJO in late 2007 and early 2008 was as large as during 1999–2002 (Fig. 3a). The convection associated with the MJO active phase resulted in a very clear decrease of the surface insolation (Fig. 6a) and an increase of the surface wind (Fig. 6b) in December and January–February. As a result, there was a surface cooling of more than 1°C in each case and a pronounced surface freshening during the second event (Fig. 6c). The January–February event is also associated with a 2°C subsurface temperature signal between 50 and 120 m (Fig. 6d) and a strong upper-ocean freshening (Fig. 6e).
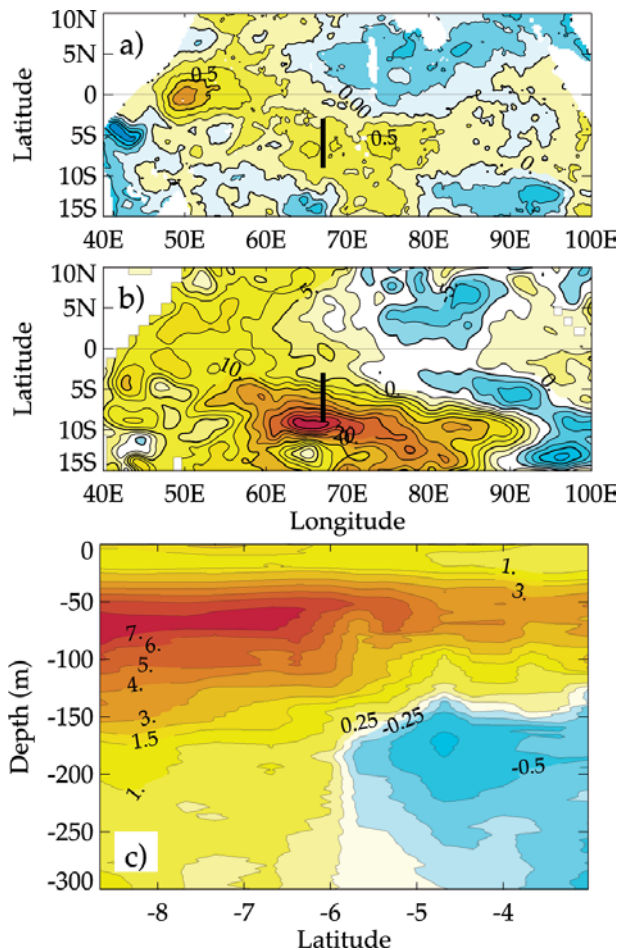
humidity, and pressure) as well as high-frequency measurements used to estimate air–sea fluxes. An instrumental suite providing measurements of the sea surface and marine boundary layer complemented the air–sea flux estimates from the mast (Minnett et al. 2001).

Detailed measurements of the upper-ocean and atmospheric evolution were collected during two long stations (from 14 January to 26 January 2007 and from 4 February to 15 February 2007) at 8°S, 67°30′E. In addition to the continuous measurements described above, we launched four radiosondes per day (at 0000, 0600, 1200, and 1800 UTC) and collected atmospheric temperature, pressure, humidity, and wind measurements up to 300 hPa for most profiles. The data were transmitted in real time and assimilated into analyses of most major operational weather centers. Upper-oceanic profiles (0–500 m), including temperature, salinity, and pressure, were performed every 20 min. One profile down to 1000 m, with additional cur-

FIG. 4. Large-scale situation during the Cirene cruise, in Jan–Feb 2007. (a) SST interannual anomaly, (b) sea level interannual anomaly, (c) temperature difference between Cirene 67°E section and World Ocean Atlas 2005 climatology (Locarnini et al. 2006). The thick line in (a) and (b) shows the location of (c). SST and sea level same as in Figs. 2, 3.

rent measurements and water sample collection, was performed every 6 h. The air–sea interaction profiler (ASIP) was deployed on several occasions during the long stations (see "The air–sea interaction profiler" sidebar for more details).

Biogeochemical measurements were also performed during the long stations. In addition to their intrinsic interest, these measurements can shed light on the physical processes in the mixed layer. For example, a surface "bloom" (sudden increase in phytoplankton) is generally indicative of upwelling or intense vertical mixing. Furthermore, chlorophyll concentration has a direct impact on light attenuation and hence on the upper ocean heat budget. Station measurements included dissolved oxygen, fluorescence (a proxy for phytoplankton), and light. Water samples were collected and have been analyzed to estimate phytoplankton and nutrient concentration.

A GLIMPSE OF 2006–07 INDIAN OCEAN DIPOLE. The timing of the Cirene cruise coincided with one of the strongest perturbations in the SCTR region over the last 10 yr (Fig. 3c). This was the consequence of a strong Indian Ocean dipole in 2006 (Fig. 2; Vinayachandran et al. 2007). As for most IODs, the SST anomalies near the equator had almost disappeared by December, but the effects in the SCTR region persisted until May 2007. In January–February, the strongest sea level anomalies were found near 10°S and a 0.5°–1°C warm SST anomaly was present in the SCTR over most of the Indian Ocean (Fig. 4). The Cirene cruise offers a unique in situ documentation of oceanis anomalies following an IOD in the SCTR region.

The measurements collected during Cirene reveal subsurface oceanic anomalies of up to 7°C along 67°E (Fig. 4c), in agreement with satellite-measured sea level data (Fig. 4b). In fact, the usual slope of the thermocline was reversed during the Cirene cruise, with the deepest thermocline at 8°S sloping up northward. The cruise-average temperature and salinity profiles at 8°S, 67°30′E confirm the strong warm anomaly down to 200 m (Fig. 5a) and a near-surface anomaly of about 1°C, consistent with satellite data estimates (Fig. 4a). The upper ocean is not only warm but also fresher than usual, with a 0.1–0.2-psu salinity anomaly in the upper 250 m (Fig. 5b). Part of this freshening can be explained by increased rain over the region in late 2006 due to the IOD (Fig. 3 in McPhaden et al. 2009; Fig. 1 in Vinayachandran et al. 2007). However, given the vertical extent of the freshening, lateral advection probably also has a role to play.

During Cirene, the surface currents were always westward (an average 0.35 m s^{-1}), with a weak southward component (Fig. 5c). The Cirene station was located in the transition region between the eastward South Equatorial Countercurrent and westward South Equatorial Current (see "The Seychelles–Chagos thermocline ridge" sidebar), and thus, in principle, in a region of weak current. The strong surface westward current during the Cirene cruise is an anomaly due to the IOD, and it is linked to the reversal of the climatological thermocline slope mentioned above. The westward current penetrated deep in the subsurface ocean, with velocities above 0.2 m s^{-1} down to 600 m (Fig. 5c). The displacement of the 0–1000-m drogued
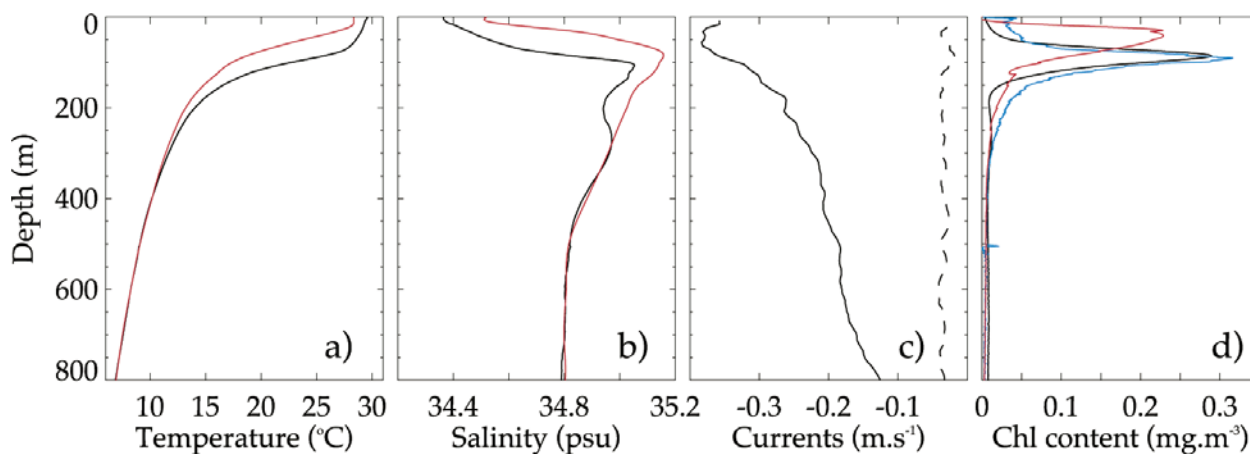

Fig. 5. Average profiles over whole cruise (14 Jan–15 Feb) at 8°S, 67°30′E. (a) Cirene temperature (black) and climatology (red). (b) Cirene salinity (black) and climatology (red). (c) Cirene zonal (continuous line) and meridional (dashed line) currents. (d) Cirene chlorophyll content (estimated from the fluorescence profile, in black). In (d), the vertical density gradients from Cirene (blue) and climatology (red) are also shown. All climatological data come from World Ocean Atlas 2005 climatology (Locarnini et al. 2006).

drifters and of the Argo profilers (parked at 1000 m) also suggested a deep strong westward flow, with consistent velocities of 0.2–0.3 m s⁻¹. An IOD thus involves a zonal redistribution of mass over the first 600 m in the SCTR region. The upper-ocean freshening could thus partly be explained by the anomalous westward transport of the fresher water from under the Inter-Tropical Convergence Zone, which lies to the east of the SCTR region. The Autonomous Temperature Line Acquisition System (ATLAS) mooring deployed during Cirene allowed monitoring the IOD-linked anomalies well beyond the end of the cruise (Fig. 6). The upper 100 m stayed unusually fresh until early July, while subsurface temperature came back to near normal during April.

During Cirene, the extreme clarity of the water was striking. Such clarity is characteristic of oligotrophic zones, that is, zones with very small near-surface phytoplankton concentration. Figure 5 shows the profile of chlorophyll concentration during the cruise. The SCTR region thus corresponds to a "typical tropical structure" (Herbland and Voituriez 1979) with a deep chlorophyll maximum (DCM). This subsurface maximum forms at the depth where both sufficient light and enhanced nutrients are available for the plankton to grow. More light is available near the surface, whereas more nutrients are available at depth because nutrients in the surface layer are usually consumed by biological activity. During Cirene, this DCM was located at an average depth of 100 m, corresponding to the thermocline level. Under climatological conditions, the thermocline is much shallower (about 30- to 50-m depth). The DCM would thus normally be expected closer to the surface where increased light availability should result in higher chlorophyll concentrations.

The IOD affected not only plankton concentration but also had a clear impact on tuna fishing. During most years, tuna purse-seine fishery catches extend eastward up to 85°E
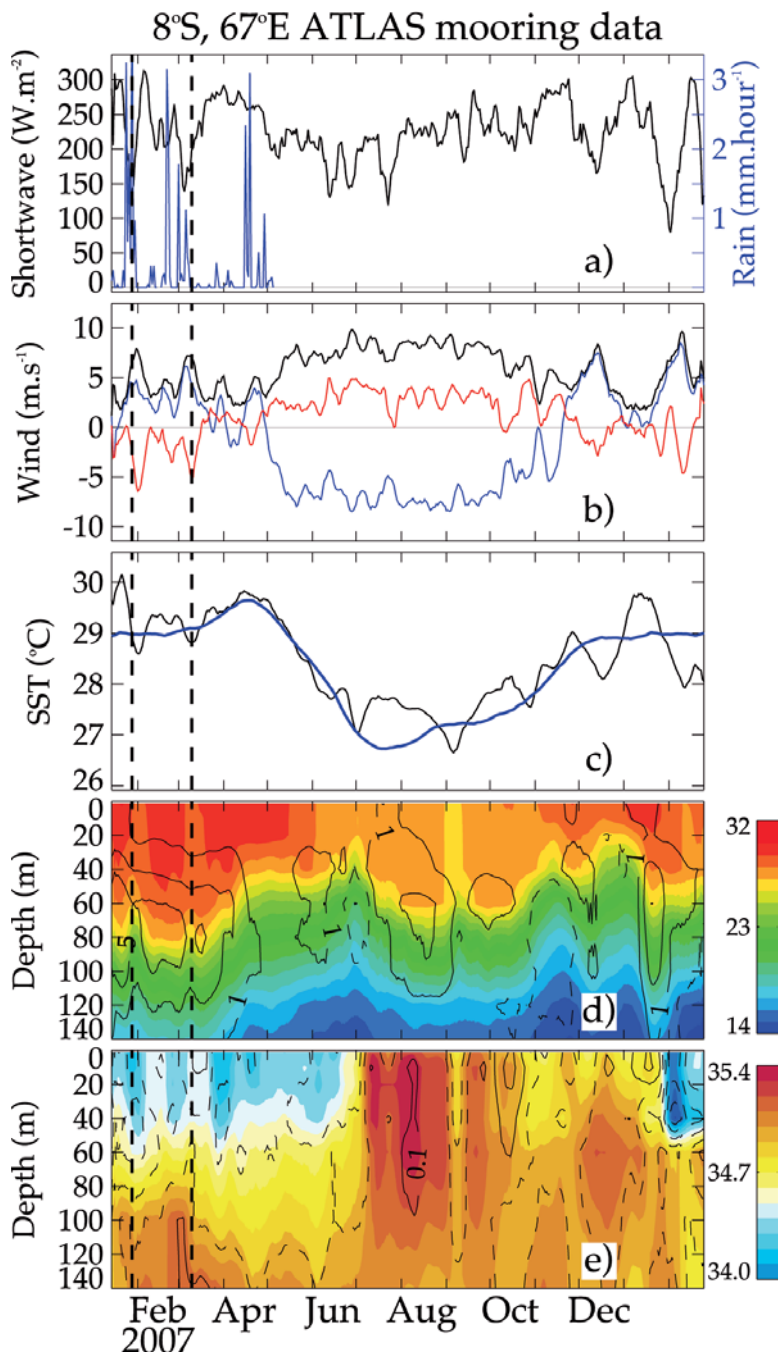

8°S, 67°E ATLAS mooring data

FIG. 6. Time series of daily parameters transmitted by the ATLAS mooring at 8°S, 67°E since its deployment during Cirene. (top to bottom) (a) Downward surface shortwave radiation (W m⁻²) and rainfall (mm h⁻¹); (b) wind speed (black), zonal wind (blue), and meridional wind (red) (m s⁻¹); (c) SST (black) and SST climatology (blue) (°C); (d) subsurface temperature (color) and anomalies (contours) (°C), and (e) subsurface salinity (color) and anomalies (contours) (psu). The SST climatology in (c) is from TMI (Wentz et al. 2000), and anomalies in (d), (e) are computed with respect to Locarnini et al. (2006).

in the SCTR region (Fig. 7a). Thermocline depth anomalies are known to affect catchability of tuna by purse seiners (Evans et al. 1981), and the 1997–98 Indian Ocean dipole had a strong impact on the tuna catch spatial distribution (Marsac and Le Blanc 1999). A deeper-than-usual thermocline provides a larger-than-normal vertical habitat of tuna, acting as a "diluting effect" on the resource and resulting in a lower vulnerability of tuna to surface fishing gear such as purse seines. The strong thermocline depth anomaly between 60° and 80°E during Cirene (Fig. 4b) probably explains why no catches by purse seiners were made at all in this longitude range during January 2007 (Fig. 7b) in this otherwise good fishing ground. In fact, we observed very little marine life during the cruise.
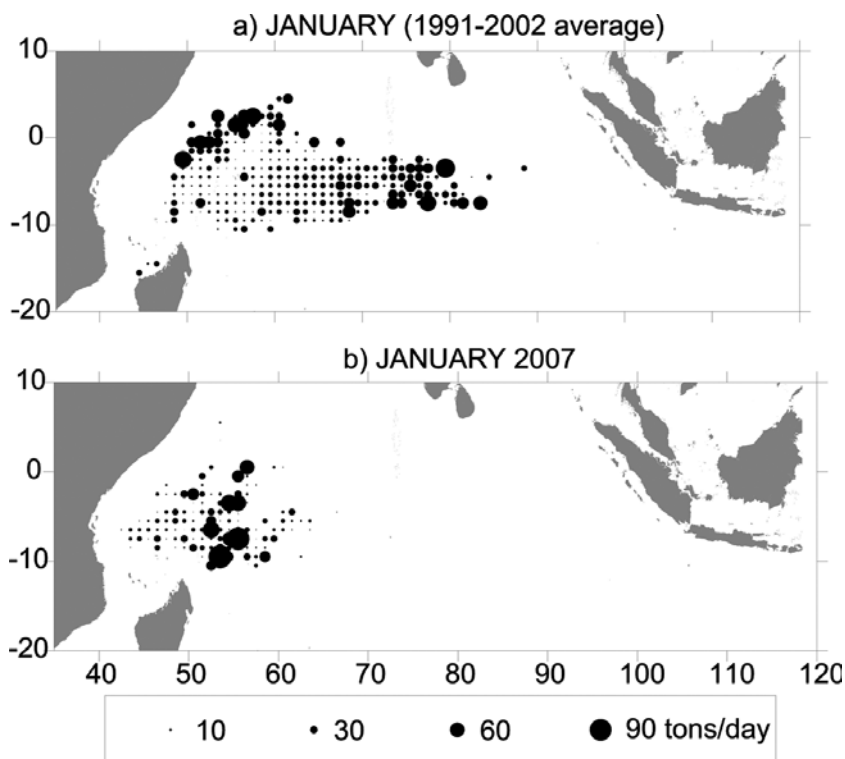
FIG. 7. (a) Average distribution of catch rate from tuna purse-seine fishery in Jan for 1991–2002. (b) Catch rate distribution for Jan 2007. The catch rates are expressed in tons per day. Notice that the usual fishing grounds for tuna between 5° and 10°S, 60° and 80°E did not witness any tuna catch in Jan 2007 due to the anomalous conditions shown in Figs. 4, 5.

INTO THE EYE OF THE TROPICAL CYCLONE.

One of the objectives of Cirene was to monitor the large SST decreases associated with the active phase of the Madden–Julian oscillation like those seen in 1999, 2000, 2001, and 2002 (Fig. 3). In this respect, 2007 was a bad year: there was no large intraseasonal SST cooling in January–February (Fig. 3a). An active phase of the MJO was, however, present over the western Indian Ocean in late December 2006 and propagated into the western Pacific, where it may have played a strong role in the unexpectedly early termination of the 2006/07 El Niño (McPhaden 2008). Convection at this time might have been facilitated by the basin-wide warming in the wake of the IOD. A suppressed phase of the Madden–Julian oscillation then set in over the SCTR region until mid-February 2007. An active phase of the MJO subsequently developed from mid-February to mid-March. Thus, the Cirene dataset mostly covers the suppressed phase of the MJO. The amplitude of the MJO variability in early 2007 at this location is as large as in 2001 (Fig. 3b), but with a much smaller SST response (Fig. 3), for reasons that will be discussed in the final section of this paper.

However, we monitored a pronounced SST cooling during Cirene (about 1.5°C), but it was of smaller spatial scale and shorter duration than those usually associated with the MJO (Fig. 6c). This cooling was associated with a tropical cyclone named Dora. There is an average of 10 tropical cyclones in the southern Indian Ocean during austral summer. There were 10 named cyclones in 2007. One of them ran almost exactly over the mooring site when it was still a tropical depression (Dora) and four more came within 800 km of the mooring between January and early April (Favio, Gamede, Indlala, and Jaya). Satellite-transmitted daily data from the ATLAS mooring clearly shows the influence of Dora and Indlala (Fig. 6). In each case there was increased wind, decreased insolation, and increased rainfall. The surface cooling was most pronounced in response to Dora (about 1.5°C) but in both cases penetrated below 100 m.

The data collected during the cruise (Figs. 8a–d) gives a more detailed view of the response to Dora. Local surface conditions during Cirene displayed four distinct phases. The first phase (from the 18–23 January) was characterized by clear skies,

strong solar radiation, and weak winds. These are surface conditions characteristic of the suppressed phase of the MJO. During this period, the oceanic mixed layer warmed by about 0.5°–0.75°C, and a strong SST diurnal cycle developed with amplitudes between 1° and 2°C. This period was also associated with a progressive moistening of the lower troposphere, associated with the upcoming Dora cyclone (Fig. 9).

The second phase (24 January–1 February) was dominated by the influence of the cyclogenesis of Dora. The last radiosondes from the first leg show
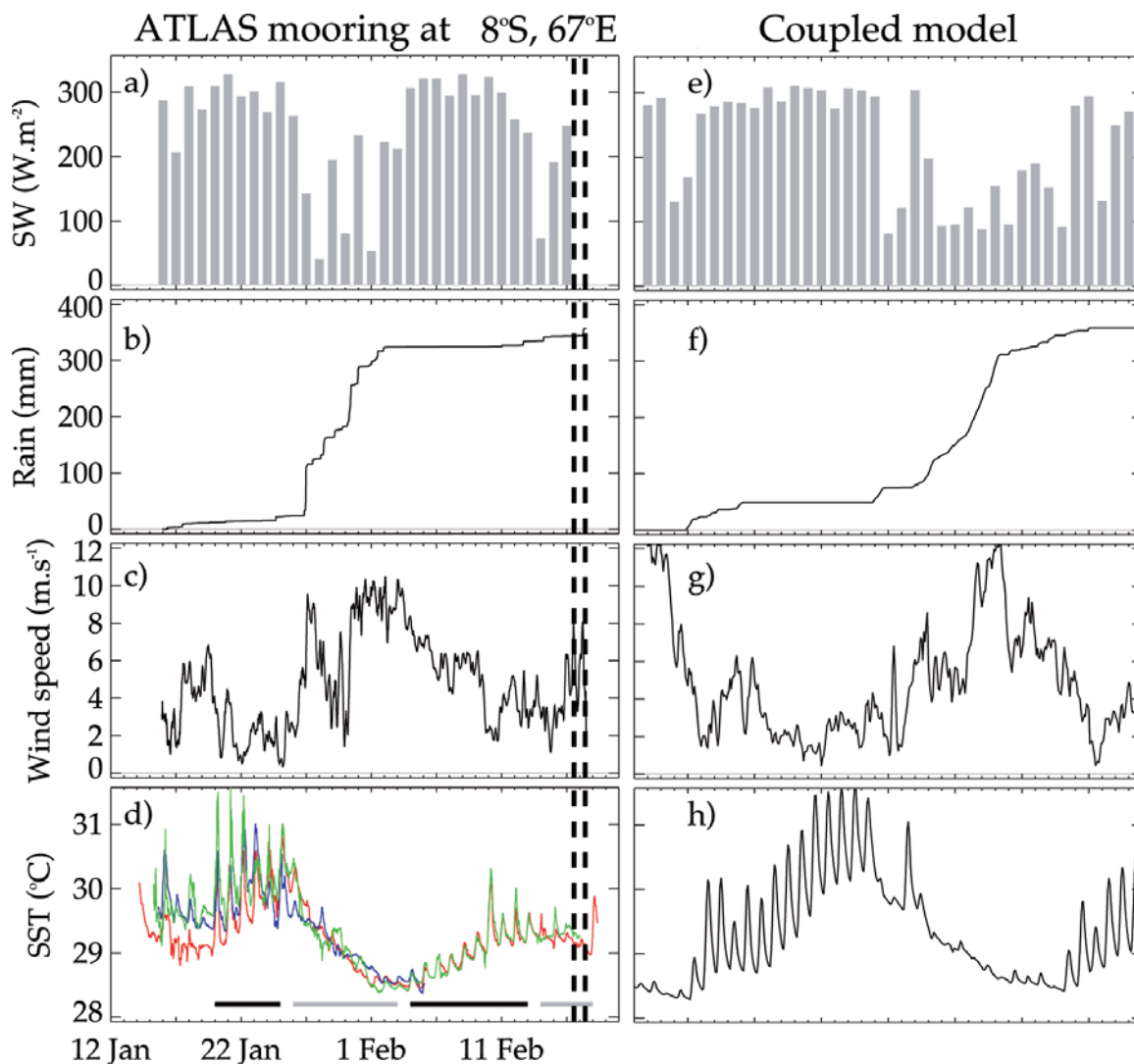
Fig. 8. (left) ATLAS mooring high-resolution (10 min) data. (a) Daily average incident shortwave flux (W m⁻²), (b) accumulated rainfall (mm), (c) wind speed with a 3-h smoothing (m s⁻¹) for the Cirene intensive observation period, (d) SST from several sources: 40-cm-depth temperature sensor from the Woods Hole Oceanographic Institution (WHOI) drifting buoys (in red and blue) and SST from ATLAS mooring (green). One of the deployment periods of the ASIP (see "ATLAS and ADCP moorings at 8°S, 67°E" sidebar; Fig. SB1) is highlighted by the vertical dashed lines. The horizontal lines at the bottom of panel (d) represent phases of surface warming (black) and surface cooling (gray). (right) Outputs from a coupled general circulation model at the Cirene location. (e) Daily average incident shortwave flux (W m⁻²), (f) cumulated rainfall (mm), (g) wind speed (m s⁻¹), (h) SST (°C). Note that the coupled model output is a sample in Jan–Feb extracted from a long simulation and that one-to-one agreement with observations cannot be expected. The features to compare are more the amplitude and time scale of the variability in the different fields, which match the observations quite well. This suggests that this coupled model is a good complementary tool to Cirene data for understanding the processes at work in the SCTR region.

a moistening of the middle troposphere, associated with developing convection (Fig. 9). Convective clouds lead to weak surface solar radiation and rain events (Figs. 8a–d). The surface wind was often between 8 and 10 m s^{-1}. The combined effect of reduced downward solar flux and increased evaporation induced strong heat losses for the upper ocean. The wind also favored vertical mixing in the upper ocean. These combined factors induced a cooling of 1.5°C in 10 days (Fig. 8d). The stronger winds also inhibited the daily formation of near-surface warm layers.

The third phase (2–11 February) corresponded to the end of the suppressed MJO period. The atmosphere was dry (Fig. 9), the surface solar flux was generally high, and the wind diminished as the cyclone migrated farther south (Figs. 8a–c). Over this period, the upper ocean gained heat again and warmed by about 0.5°C. Some weak diurnal cycle also developed. The fourth phase, at the end of the cruise, is influenced by Cyclone Favio and the return of MJO active conditions. It is associated with increased humidity in the lower and midtroposphere (Fig. 9), decreased solar radiation, some rain events, slightly stronger winds, and a slight SST cooling (Figs. 8a–d).

While Cirene provided data close to the cyclones during their formation, the Vasco balloons came even closer when the cyclones were fully formed. Two Aeroclippers converged into the eye of Dora (Fig. 10a), enduring wind speeds above 40 m s^{-1}, and stayed confined within the eye for more than a week (Duvel et al. 2009). This gave for the first time a direct estimate of the surface radial and tangential winds as a function of the distance from the eye. Pressurized balloons were also captured by Tropical Cyclones Dora and Gamede. For Gamede (Fig. 10b), one pressurized balloon stayed confined for around 12 revolutions near the maximum wind with almost no radial speed and tangential speed between 30 and 40 m s^{-1}. These results show that both pressurized and Aeroclipper balloons can measure inside tropical cyclones, giving a new in situ measurement capability, in particular, for the validation of satellite estimate of the cyclone intensity.

SCALE INTERACTIONS. We have seen that the SCTR region hosts variability at many different temporal and spatial scales. The IOD is basin scale at interannual time scales and the MJO is basin scale at intraseasonal time scales. Cyclones, at synoptic and weekly scales, are also strong contributors to the variability in this region. However, as suggested above, there is variability at an even finer scale (e.g., the strong diurnal cycle when the wind is weak). While having very different scales, those phenomena can interact with each other. For example, cyclones are influenced by SCTR interannual variability (Xie et al. 2002) and the MJO (Bessafi and Wheeler 2006). In this section, we will illustrate how some of the finescale observed during the cruise might be relevant for longer-lived phenomena like the MJO or IOD.
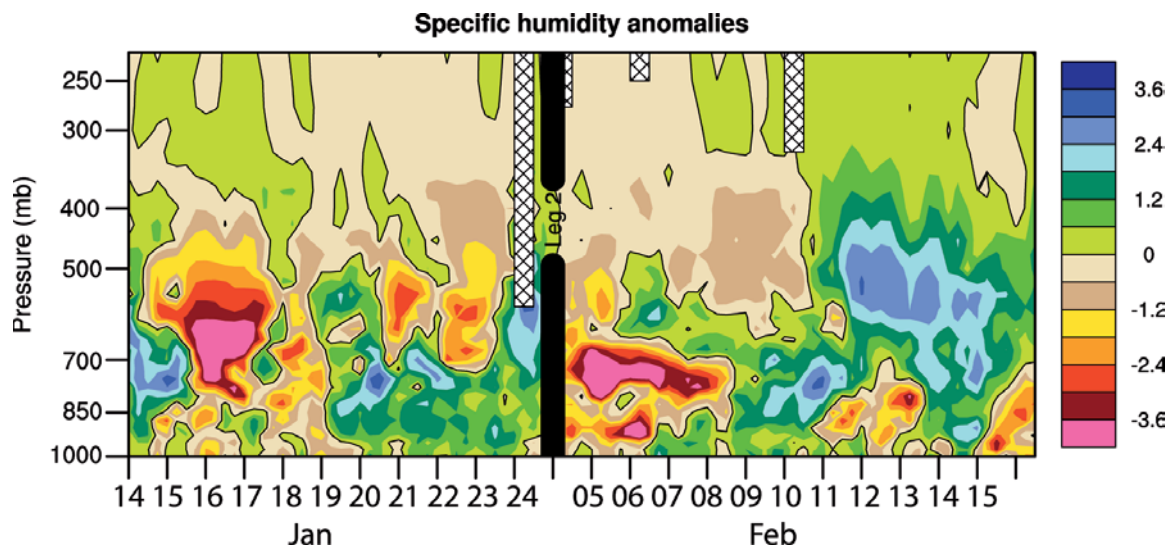

FIG. 9. Pressure–time section of specific humidity anomalies (g kg^{-1}) at 8°S, 67°30′E from Cirene radiosondes (anomalies with respect to the average over the whole cruise). The gap between the two legs is marked with the thick black line. The cross-hatched bars indicate missing data. Moistening associated with Cyclone Dora is seen at the end of leg 1, and moistening associated to Cyclone Favio and to the return of active MJO conditions is seen at the end of leg 2.

During convectively suppressed periods, low surface wind leads to reduced vertical mixing. Incident solar flux generates stable stratification at the surface, which results in a strong diurnal variation of the SST (Ward 2006; Stramma et al 1986; Fig. 8d). Because of the asymmetry of the mixing processes (heating concentrated in the first meter during the day, and cooling spread over the thickness of the mixed layer during the night), diurnal warm layers induce a higher SST than that expected from daily average air–sea heat fluxes. During the convectively active phase of the MJO, there are strong surface winds and no warm layer can form. As a result, diurnal warm layers tend to increase the amplitude of intraseasonal perturbations of the SST (e.g., Shinoda and Hendon 1998; Bernie et al. 2005). These diurnal warm layers influence the atmospheric variability from diurnal to intraseasonal time scales and improve the MJO predictability in a GCM (Woolnough et al. 2007). Here, a similar mechanism is at play but in relation to cyclone development (Fig. 8; see also the previous section), which raises the question of the role of these warm layers in the cyclogenesis. The example of the diurnal cycle illustrates how important finescale mechanisms could potentially be to understanding variability at the scale of the MJO or IOD.

Atmospheric profiles (Fig. 9) showed dry layers around 700 hPa at the beginning of both legs. These were probably related to dry-air intrusion produced by subsiding upper-level extratropical air. These dry intrusions were previously observed in the western Pacific (Mapes and Zuidema 1996), in the Indian Ocean (Zachariasse et al. 2001), and over West Africa (Roca et al. 2005). A dry layer in the lower troposphere can inhibit both deep convection (Mapes and Zuidema 1996) and the ability of tropical cyclones to strengthen (Dunion and Velden 2004). How these dry intrusions interact with cyclogenesis or the MJO has to be explored.

In the ocean, finescale mechanisms may be important to the understanding of the upper-ocean heat budget at longer time scales. Time series from the station at 8°S, 67°30′E (Fig. 11) and from the ATLAS mooring show a strong tidal variability in the thermocline with a 12-h time scale. Tides usually involve a movement of the whole water column. However, in regions with rugged bottom topography like the area of the cruise, internal oceanic waves can be generated by tides and travel upward toward the thermocline. The current shear they generate there results in enhanced turbulence and can affect the rate of exchange between mixed layer and thermocline water, thus impacting the upper-ocean heat balance. Preliminary computations suggest that these "internal tides" induce a twofold increase of mixing in the thermocline, which probably needs to be considered to close the upper-ocean heat budget over long time scales. Figure 11 also shows al-
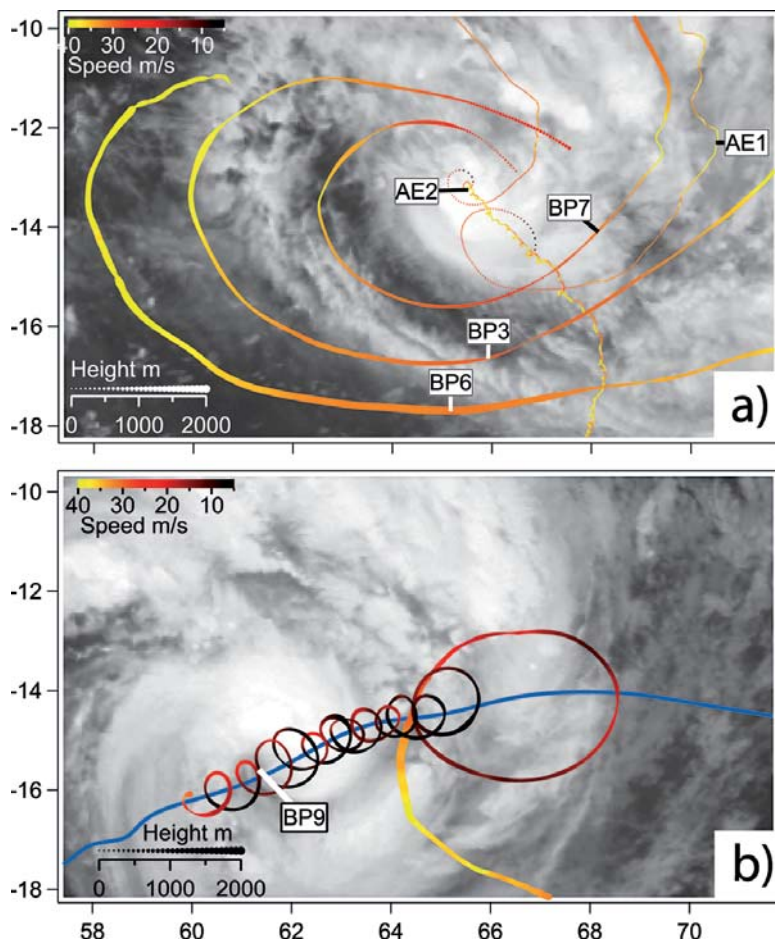

FIG. 10. Trajectories of Vasco balloons in the vicinity of two cyclones, with background images from Meteosat satellite. (a) Tropical Cyclone Dora (image from 30 Jan), with two Aeroclippers (AE1 and AE2) converging into the eye, and three pressurized balloons (BP3, BP6, and BP7) attracted by the cyclone convergence, (b) Cyclone Gamede (image from 23 Feb) with one pressurized balloon (BP9) converging into the eye. Note that in all cases, balloons attained velocities above 30 m s⁻¹.
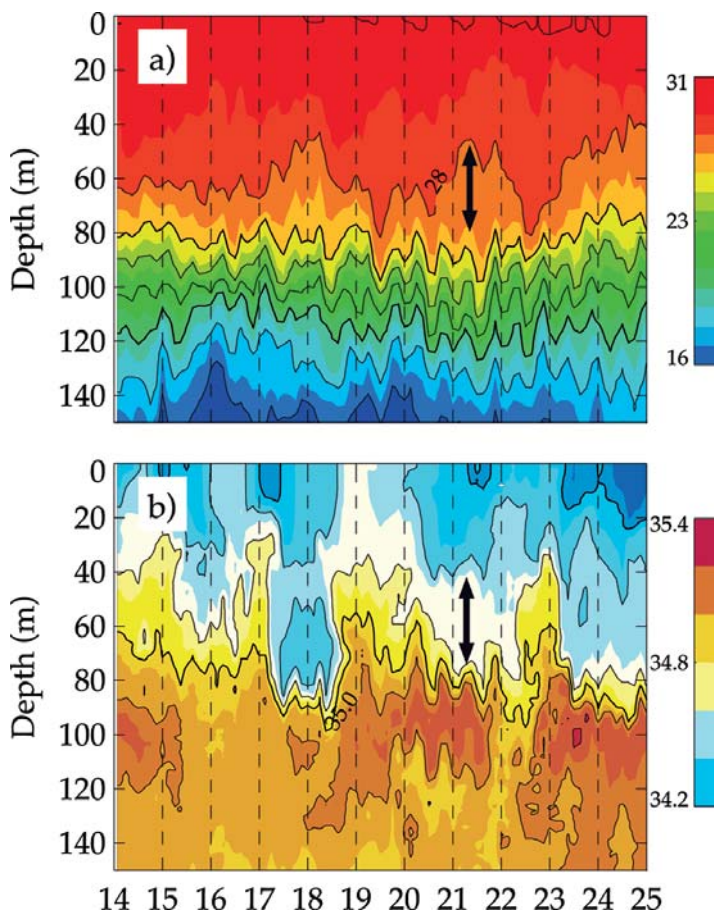
FIG. 11. Time–vertical section of the upper 150 m of the Cirene 8°S, 67°30′E leg 1 long stations: (a) temperature and (b) salinity. The profiles (with three profiles per hour most of the time) have been averaged into 3-h slots. The arrow indicates the formation of a 30-m-thick homogeneous layer in salinity and temperature, probably linked to interleaving of two different water masses (see "Scale interactions" for more details).

the SST anomalies, because they influence the cyclone distribution near Madagascar (Xie et al. 2002) and the rainfall over the western Ghats of India during the following monsoon (Vecchi and Harrison 2004; Izumo et al. 2008). In 2007, however, the number of tropical cyclones was not above normal. On the other hand, rainfall over the western Ghats of India (inside 14°–20°N, 72°–76°E) during June–August was 25 cm above the climatological value of 91 cm. Thus, 2007 might be a good year to test the dynamical mechanisms proposed by Izumo et al. (2008) using atmospheric general circulation models.

We also observed the ocean perturbation during and following the genesis of Cyclone Dora. These data might be useful for understanding the role of air–sea interaction in the cyclogenesis process over this region of the Indian Ocean. Important physical processes playing a role in scale interaction were also observed during the experiment. In particular, we observed small-scale oceanic variability (near-surface diurnal cycle, internal tides; interleaving) that affects the evolution of the ocean thermal structure at longer time scales through increased mixing. In the atmosphere, the radiosondes will allow us to study the role of the surface diurnal warm layer in the evolution of the boundary layer structure. Also, the large-scale origin of the dry air that inhibited the local convection at the beginning of each Cirene leg will be studied using meteorological analyses complemented by the Vasco balloon measurements.

We did not observe a strong cooling associated with the MJO activity in early 2007, although this MJO activity was not negligible. Previous studies (e.g., Harrison and Vecchi 2001; Duvel et al. 2004) have suggested that the thermocline depth modulates the SST response in the SCTR region. However, most years since 2003 have been associated with a deeper SCTR and a higher sea level than normal (Fig. 2; Lee

ternating patches of saltier/warmer and fresher/cooler water between 40 and 80 m. The presence of two neighboring density-compensated water masses can be conducive to thermohaline intrusions, double diffusive mixing, and the formation of vertically mixed regions in oceanic profiles (see Ruddick and Richards 2003 for a review). Many examples of formation of vertically mixed regions can be seen in the Cirene dataset, with the clearest starting on 20 January near 55 m. After 2 days, this resulted in a 30-m homogeneous temperature and salinity slice between 50 and 80 m (Fig. 11). Preliminary analyses also suggest that these processes have a significant impact on mixing and might need to be considered when examining the heat budget over longer time scales.

ONGOING WORK AND PERSPECTIVES.

The Vasco–Cirene data, in combination with satellite data and modeling studies, comprise a new set of measurements to study the variability in the SCTR region at various time scales. In particular, the Cirene data document interannual anomalies following an IOD in the SCTR region and the processes that account for them. It will be interesting to understand what causes

and McPhaden 2008), which might have made the SST less responsive to atmospheric perturbations. The amplitude of the MJO convective variability in early 2007 at this location was as large as in 2001, but with a much smaller SST response. This could also be due to the anomalously deep thermocline linked to the 2006/07 IOD. In a modeling environment, with the Cirene data as a reference, we will be able to test how the thermocline depth affects the response of the upper ocean to cyclones and to the MJO.

Another set of questions to address is the relative influence of the local (SST; boundary layer charac-

THE AIR–SEA INTERACTION PROFILER

The surface ocean diurnal cycle is an important focus of Cirene, in particular because of its contribution to the MJO-induced SST signature. This diurnal cycle has a very fine vertical scale (1–3 m), which is difficult to measure near ships because of mixing induced by the hull. The ASIP is an autonomous profiling instrument designed to provide high-resolution upper-ocean measurements. ASIP's design is based on the successful Skin Depth Experiment (SkinDeEp) profiler (Ward et al. 2004). The Cirene cruise was the first time ASIP was deployed in the open ocean.

The photograph in Fig. SB1 was taken during Cirene and shows the instrument at about 5-m depth. Autonomous profiling is accomplished with a thruster (at the bottom of the instrument), which submerges ASIP to a programmed depth. Once this depth is reached, the thruster switches off, and the positively buoyant instrument ascends to the surface acquiring data. ASIP can profile from a maximum depth of 100 m to the surface, allowing both mixed layer and near-surface measurements to be conducted. During Cirene, ASIP was equipped with high-resolution (~1-cm vertical resolution) measurements of temperature, salinity, and small-scale turbulence. With these sensors, ASIP had

autonomy of about 300 profiles. It transmits its position and vital statistics through Iridium.

Figure SB1 shows an example of 20 h of salinity data from ASIP. Wind speeds were moderate (<5 m s⁻¹), although quite variable during the few days surrounding this deployment, with some wind bursts to 10 m s⁻¹ (Fig. 8). The ASIP data showed a shallow (~ 1 m) freshening associated with a first nighttime rain event. Nighttime convective overturning quickly mixed down the surface freshwater lens. The rain gauge on the R/V *Suroît* recorded a fairly strong rain event just after sunrise, associated with a sharp decrease in air temperature. A surface freshwater lens formed after this rain event and remained quite shallow (~10 m), probably because of weak winds. This example demonstrates the ability of ASIP to perform fine vertical-scale measurements near the ocean surface. The ASIP dataset (in particular, the microstructure measurements) will be precious to evaluate the finescale structure of freshwater penetration into the upper ocean after a rain event and will complete usefully the previous studies from the Coupled Ocean–Atmosphere Response Experiment on this topic (e.g., Brainerd and Gregg 1997).
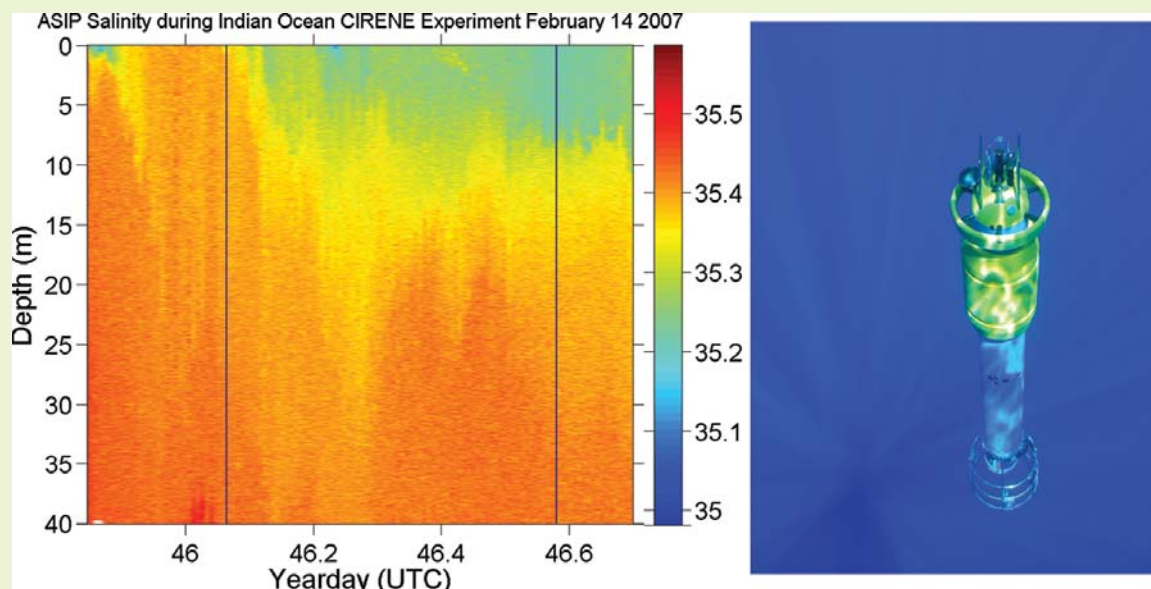

FIG. SB1. (left) Time–depth section of upper ocean salinity measured by ASIP. The measurement period was 0040–2100 (LT) 15 Feb. The two vertical lines indicate sunrise (0550) and sunset (1810). (right) Underwater photograph of ASIP. Note the extreme clarity of the water.

teristics) and large-scale (e.g., MJO- or IOD-driven subsidence or low-level convergence) conditions for the initiation of convection. Is the formation of the very high SST and strong diurnal cycle observed during the first leg linked to large-scale subsidence? Does the cooling resulting from Cyclone Dora interact with the MJO cycle?

There should be a two-way interaction between modeling and Vasco–Cirene measurements. First, process studies are a stringent test on the model to see if they can reproduce the important physical mechanisms at work. Second, if they do, the models can be used as a complement to the data to understand the processes at work. Figure 8 illustrates that an upgraded version of the Scaled Interaction Experiment-FRCGC (SINTEX-F) coupled general circulation model (e.g., Masson et al. 2005) with 1-m vertical resolution near the surface can reproduce some of the processes that were observed during Cirene. The alternate periods of active convection (strong wind, rainfall, low insolation, and decreasing SST) and clear skies (with rising SST and strong diurnal cycle) are qualitatively well reproduced. Such coupled models will be useful to design sensitivity experiments to test hypotheses stimulated by the analysis of Cirene data.

The World Climate Research Program CLIVAR Indian Ocean panel has highlighted the important processes in the SCTR region and has called for observations in this area (CLIVAR/GOOS IOP et al. 2006). The recent Cirene and Mirai Indian Ocean cruise for the study of MJO-convection onset (MISMO; Yoneyama et al. 2008) cruises will contribute to address some of the important questions, but sustained observations in the region are needed to better characterize the variability and to understand the processes governing them. The ATLAS mooring at 8°S, 67°E, as part of RAMA (McPhaden et al. 2009), is an important first step. International collaboration for a new experiment in the region in 3 or 4 yr from now, building on the Vasco–Cirene and MISMO concepts, is also envisaged; it would provide an opportunity to contribute again to sustained observations in that important region.

REFERENCES

Annamalai, H., P. Liu, and S.-P. Xie, 2005: Southwest Indian Ocean SST variability: Its local effect and remote influence on Asian monsoons. *J. Climate,* **18,** 4150–4167.

——, H. Okajima, and M. Watanabe, 2007: Possible impact of the Indian Ocean SST on the Northern Hemisphere circulation during El Niño. *J. Climate,* **20,** 3164–3189.

Bernie, D.J., S. J. Woolnough, J.M. Slingo, and E. Guilyardi, 2005: Modeling diurnal and intraseasonal variability of the ocean mixed layer. *J. Climate,* **18,** 1190–1202.

Bessafi, M., and M. C. Wheeler, 2006: Modulation of south Indian Ocean tropical cyclones by the Madden–Julian oscillation and convectively coupled equatorial waves. *Mon. Wea. Rev.,* **134,** 638–656.

Brainerd, K. E., and M.C. Gregg, 1997: Turbulence and stratification on the Tropical Ocean–Global Atmosphere Coupled Ocean–Atmosphere Response Experiment microstructure pilot cruise. *J. Geophys. Res.,* **102,** 10 437–10 455.

CLIVAR/GOOS Indian Ocean Panel, and Collaborators, 2006: Understanding the role of the Indian Ocean in the climate system—Implementation plan for sustained observations. ICPO Publication Series No. 100, GOOS Rep. 152, International CLIVAR Project Office, 76 pp.

Dunion, J. P., and C. S. Velden, 2004: The impact of the Saharan air layer on Atlantic tropical cyclone activity. *Bull. Amer. Meteor. Soc.,* **85,** 353–365.

Dupuis, H., C. Guérin, D. Hauser, W. Weill, P. Nacass, W. Drennan, S. Cloché, and H. Graber, 2003: Impact

of flow distortion corrections on turbulent fluxes estimated by the inertial-dissipative method during FETCH experiment on R/V *L'Atalante. J. Geophys. Res.,* **108,** 8064, doi:10.1029/2001JC001075.

Duvel, J. P., and J. Vialard, 2007: Indo-Pacific sea surface temperature perturbations associated with intraseasonal oscillations of the tropical convection. *J. Climate,* **20,** 3056–3082.

——, R. Roca, and J. Vialard, 2004: Ocean mixed layer temperature variations induced by intraseasonal convective perturbations over the Indian Ocean. *J. Atmos. Sci.,* **61,** 1004–1023.

——, C. Basdevant, H. Bellenger, G. Reverdin, A. Vargas, and J. Vialard, 2009: The Aeroclipper—A new device to explore convective systems and cyclones. *Bull. Amer. Meteor. Soc.,* **90,** 63–71.

Evans, R. H., D. R. McLain, and R. A. Bauer, 1981: Atlantic skipjack tuna: Influences of mean environmental conditions on their vulnerability to surface fishing gear. *Mar. Fisheries Rev.,* **43,** 1–11.

Fieux, M., and C. Lévy, 1983: Seasonal observations in the western Indian Ocean. *Hydrodynamics of the Equatorial Ocean,* J. C. J. Nihoul, Ed., Elsevier, 17–29.

Gould, J., and Argo Steering Team, 2004: Argo profiling floats bring new era of in situ ocean observations. *Eos, Trans. Amer. Geophys. Union,* **85,** 179–191.

Harrison, D.E., and G.A. Vecchi, 2001: January 1999 Indian Ocean cooling event. *Geophys. Res. Lett.,* **28,** 3717–3720.

Herbland, A., and B. Voituriez, 1979: Hydrological structure analysis for estimating the production in the tropical Atlantic Ocean. *J. Mar. Res.,* **37,** 87–101.

Hermes, J. C., and C. J. C. Reason, 2008: Annual cycle of the south Indian Ocean (Seychelles–Chagos) thermocline ridge in a regional ocean model. *J. Geophys. Res.,* **113,** C04035, doi:10.1029/2007JC004363.

Izumo, T., C. de Boyer Montegut, J-J. Luo, S. K. Behera, S. Masson, and T. Yamagata, 2008: The role of the western Arabian Sea upwelling in Indian monsoon rainfall variability. *J. Climate,* **21,** 5603–5623..

Jury, M., B. Pathack, and B. Parker, 1999: Climatic determinants and statistical prediction of tropical cyclone days in the southwest Indian Ocean. *J. Climate,* **12,** 1738–1755.

Klein, S. A., B. J. Soden, and N.-C. Lau, 1999: Remote sea surface temperature variations during ENSO: Evidence for a tropical atmospheric bridge. *J. Climate,* **12,** 917–932.

Lau, N.-C., and M. J. Nath, 2000: Impact of ENSO on the variability of the Asian–Australian monsoons as simulated in GCM experiments. *J. Climate,* **13,** 4287–4309.

Lee, T., and M. J. McPhaden, 2008: Decadal phase change in large-scale sea level and winds in the Indo-Pacific region at the end of the 20th century. *Geophys. Res. Lett.,* **35,** L01605, doi:10.1029/2007GL032419.

Liebmann, B., and C. A. Smith, 1996: Description of a complete (interpolated) outgoing longwave radiation dataset. *Bull. Amer. Meteor. Soc.,* **77,** 1275–1277.

Liebmann, B., H. H. Hendon, and J. D. Glick, 1994: The relationship between tropical cyclone of the western Pacific and Indian Oceans and the Madden–Julian oscillation. *J. Meteor. Soc. Japan,* **72,** 401–412.

Locarnini, R. A., A. V. Mishonov, J. I. Antonov, T. P. Boyer, and H. E. Garcia, 2006: *Temperature.* Vol 1, *World Ocean Atlas 2005,* NOAA Atlas NESDIS 61, 182 pp.

Madden, R. A., and P. R. Julian, 1994: Observations of the 40–50 day tropical oscillation—A review. *Mon. Wea. Rev.,* **122,** 814–837.

Maloney, E. D., and A. H. Sobel 2004: Surface fluxes and ocean coupling in the tropical intraseasonal oscillation. *J. Climate,* **17,** 4368–4386.

Mapes, B. E., and P. Zuidema, 1996: Radiative-dynamical consequences of dry tongues in the tropical troposphere. *J. Atmos. Sci.,* **53,** 620–638.

Marsac, F., and J.-L. Le Blanc, 1999: Oceanographic changes during the 1997–1998 El Niño in the Indian Ocean and their impact on the purse Seine fishery. *Proc. First IOTC Working Party on Tropical Tunas,* Mahe, Seychelles, IOTC, 147–157.

Masson, S., and Coauthors, 2005: Impact of barrier layer on winter-spring variability of the southeastern Arabian Sea. *Geophys. Res. Lett.,* **32,** L07703, doi:10.1029/2004GL021980.

Masumoto, Y., and G. Meyers, 1998: Forced Rossby waves in the southern tropical Indian Ocean. *J. Geophys. Res.,* **103,** 27 589–27 602.

McCreary, J. P., P. K. Kundu, and R. L. Molinari, 1993: A numerical investigation of dynamics, thermodynamics and mixed-layer processes in the Indian Ocean. *Prog. Oceanogr.,* **31,** 181–244.

McPhaden, M. J., 1999: Genesis and evolution of the 1997–1998 El Niño. *Science,* **283,** 950–954.

——, 2008: Evolution of the 2006–07 El Niño: The role of intraseasonal to interannual time scale dynamics. *Adv. Geosci.,* **14,** 219–230.

——, and Coauthors, 2009: RAMA: Research moored array for African–Asian–Australian Monsoon Analysis and prediction. *Bull. Amer. Meteor. Soc.,* in press.

Meyers, G., and R. Boscolo, 2006: The Indian Ocean observing system (IndOOS). *CLIVAR Exchanges,* No. 4, International CLIVAR Project Office, Southampton, United Kingdom, 2–3.

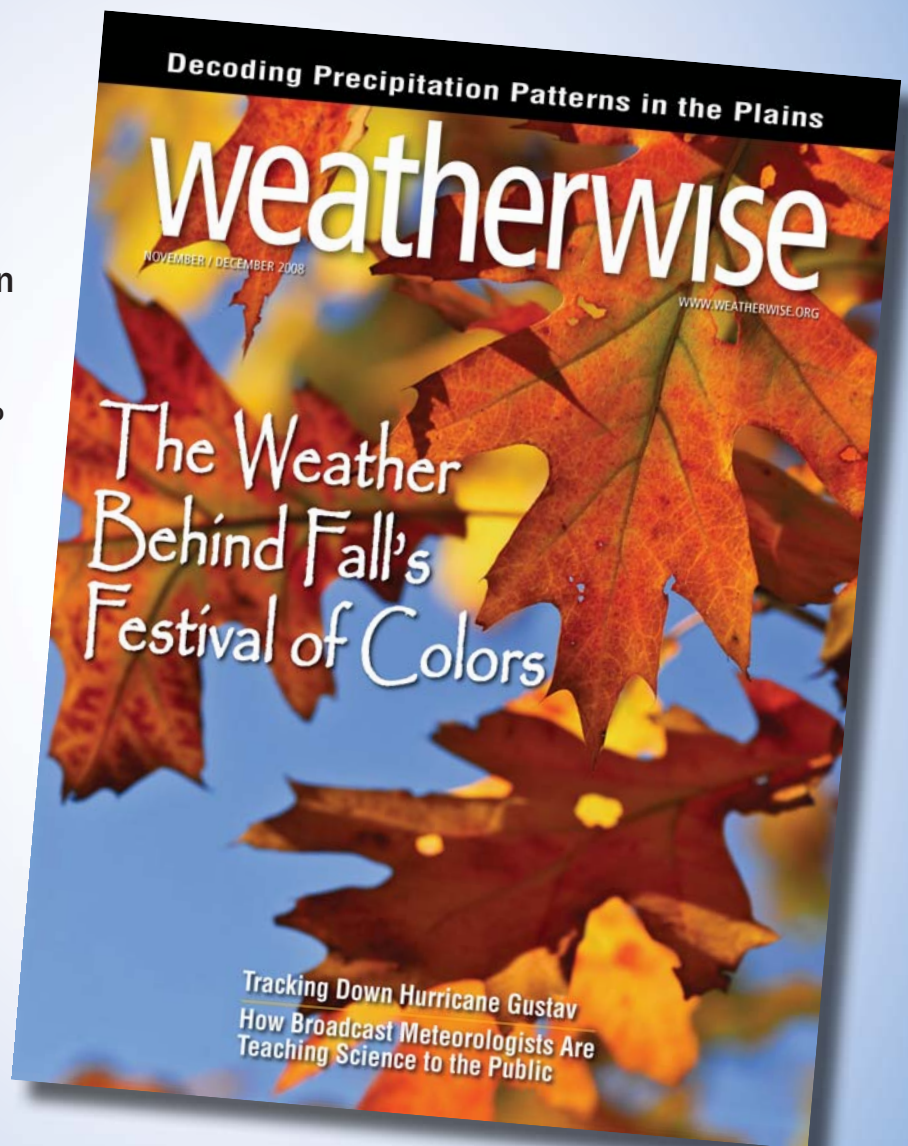Minnett, P. J., R. O. Knuteson, F. A. Best, B. J. Osborne, J. A. Hanafin, and O. B. Brown, 2001: The Marine-

Atmosphere Emitted Radiance Interferometer: A high-accuracy, seagoing infrared spectroradiometer. *J. Atmos. Oceanic Technol.,* **18,** 994–1013.

Murtugudde, R., J. P. McCreary, and A. J. Busalacchi, 2000: Oceanic processes associated with anomalous events in the Indian Ocean with relevance to 1997–1998. *J. Geophys. Res.,* **105,** 3295–3306.

Plotnikov, V. A., 1986: Temperature-salinity and dynamical structure of waters in the subequatorial regions of the Indian Ocean. *Ecological Systems in Active Dynamical Zones of the Indian Ocean* (in Russian), T. S. Petipa, Ed., Naukova Dumka, 18–46.

Reverdin, G., and M. Fieux, 1987: Sections in the western Indian Ocean—Variability in the temperature structure. *Deep-Sea Res.,* **34,** 601–626.

Roca, R., J. P. Lafore, C. Piriou, and J. L. Redelsperger, 2005: Extratropical dry-air intrusions into the West African monsoon midtroposphere: An important factor for the convective activity over the Sahel. *J. Atmos. Sci.,* **62,** 390–407.

Ruddick, B., and K. Richards, 2003: Oceanic thermohaline intrusions: Observations. *Prog. Oceanogr.,* **56,** 499–527.

Saji, N. H., B. N. Goswami, P. N. Vinayachandran, and T. Yamagata, 1999: A dipole mode in the tropical Indian Ocean. *Nature,* **401,** 360–363.

——, S.-P. Xie, and C.-Y. Tam, 2006: Satellite observations of intense intraseasonal cooling events in the tropical south Indian Ocean. *Geophys. Res. Lett.,* **33,** L14704, doi:10.1029/2006GL026525.

Schott, F., and J. P. McCreary, 2001: The monsoon circulation of the Indian Ocean. *Prog. Oceanogr.,* **51,** 1–123.

——, M. Dengler, and R. Schoenefeldt, 2002: The shallow overturning circulation of the Indian Ocean. *Prog. Oceanogr.,* **53,** 57–103.

Shinoda, T., and H. H. Hendon, 1998: Mixed layer modeling of intraseasonal variability in the tropical Western Pacific and Indian Oceans. *J. Climate,* **11,** 2668–2685.

Stramma, L., P. Cornillon, R. A. Weller, J. F. Price, and M. G. Briscoe, 1986: Large diurnal sea surface temperature variability: Satellite and in situ measurements. *J. Phys. Oceanogr.,* **16,** 827–837.

Vecchi, G. A., and D. E. Harrison, 2004: Interannual Indian rainfall variability and Indian Ocean sea surface temperature anomalies. *Earth Climate: The Ocean-Atmosphere Interaction, Geophys. Monogr.,* Vol. 147, Amer. Geophys. Union, 247–260.

Vialard, J., G. Foltz, M. McPhaden, J.-P. Duvel, and C. de Boyer Montégut, 2008: Strong Indian Ocean cooling associated with the Madden–Julian Oscillation in late 2007 and early 2008. *Geophys. Res. Lett.,* **35,** L19608, doi:10.1029/2008GL035238.

Vinayachandran, P. N., S. Iizuka, and T. Yamagata, 2002: Indian Ocean dipole mode events in an ocean general circulation model. *Deep-Sea Res. II,* **49,** 1573–1596.

——, J. Kurian, C. P. Neema, 2007: Indian Ocean response to anomalous conditions in 2006. *Geophys. Res. Lett.,* **34,** L15602, doi:10.1029/2007GL030194.

Waliser, D. E., K. M. Lau, and J.-H. Kim, 1999: The influence of coupled sea surface temperatures on the Madden–Julian oscillation: A model perturbation experiment. *J. Atmos. Sci.,* **56,** 333–358.

Ward, B., 2006: Near-surface ocean temperature. *J. Geophys. Res.,* **111,** C02005, doi:10.1029/2004JC002689.

——, R. Wanninkhof, P. J. Minnett, and M. Head, 2004: SkinDeEp: A profiling instrument for upper decameter sea surface measurements. *J. Atmos. Oceanic Technol.,* **21,** 207–222.

Webster, P. J., A. M. Moore, J. P. Loschnigg, and R. R. Leben, 1999: Coupled oceanic–atmospheric dynamics in the Indian Ocean during 1997–98. *Nature,* **401,** 356–360.

Wentz, F. J., C. Gentemann, D. Smith, and D. Chelton, 2000: Satellite measurements of sea surface temperature through clouds. *Science,* **288,** 847–850.

Woolnough, S. J., F. Vitart, and M. A. Balmaseda, 2007: The role of the ocean in the Madden–Julian oscillation: Implications for MJO prediction. *Quart. J. Roy. Meteor. Soc.,* **133,** 117–128.

Xie, S.-P., H. Annamalai, F. A. Schott, and J. P. McCreary, 2002: Structure and mechanisms of South Indian climate variability. *J. Climate,* **15,** 864–878.

Yokoi, T., T. Tozuka, and T. Yamagata, 2008: Seasonal variation of the Seychelles Dome. *J. Climate,* **21,** 3740–3754.

Yoneyama, K., and Coauthors, 2008: MISMO field experiment in the equatorial Indian Ocean. *Bull. Amer. Meteor. Soc.,* **89,** 1889–1903.

Yu, W., B. Xiang, L. Liu, and N. Liu, 2005: Understanding the origins of interannual thermocline variations in the tropical Indian Ocean. *Geophys. Res. Lett.,* **32,** L24706, doi:10.1029/2005GL024327.

Zachariasse, M., H. G. J. Smit, P. F. J. van Velthoven, and H. Kelder, 2001: Cross-troposphere and interhemispheric transports into the tropical free troposphere over the Indian Ocean. *J. Geophys. Res.,* **106,** 28 441–28 452.

Zhang, C., 2005: Madden–Julian Oscillation. *Rev. Geophys.,* **43,** RG2003, doi:10.1029/2004RG000158.